JOURNAL OF COMPUTATIONAL PHYSICS 1, 406–432 (1967)

Numerical Calculations of Multidimensional and Unsteady Flows by the Method of Characteristics

HARRY SAUERWEIN

Aerospace Corporation,
San Bernardino, California 92402

ABSTRACT

The analytic and numerical procedures necessary to write a general method of characteristics computer code are presented. The theory of characteristics is applied to the partial differential equations of an inviscid fluid, the geometry of the characteristics is determined, a procedure for finite-differencing the compatibility equations is developed and the stability of the procedure is analyzed. The details of the finite-difference network and of a successful organization of the network to calculate complete flow fields are presented. The flow between a detached shock wave and the surface of a two-dimensional body in unsteady motion has been calculated. The results of several calculations of specific body motions are presented. From the results it is concluded that practical calculations of multidimensional unsteady flows can be accomplished with an extensive coding effort and a reasonable amount of computer time.

I. INTRODUCTION AND NOTATION

The extension of the method of characteristics to the calculation of problems involving more than two independent variables has been considered for many years. Not until the last five or six years, however, have digital computers been available with the speed and capacity for attempting three independent variable problems. The history of the development of multidimensional characteristic methods is outlined and an extensive list of references is given in [1] and [2]. Some recently published papers on the method are [3]–[6]. The first attempts at performing multidimensional characteristic calculations have been, understandably, oriented toward solving rather specific flow configurations rather than developing a general approach which might be used on most problems of interest. This paper presents the results of new work in the development of a practical and

general method of characteristics which can be applied to problems involving more than two independent variables.

Before going into the details of the method of characteristics, a brief discussion contrasting the method of characteristics with "standard finite difference methods" [7] is in order. First of all, the method of characteristics uses a characteristic or curvilinear net while the standard finite difference approach uses a rectangular net and usually uses artificial viscosity [8] or a particular choice of differencing [9]. These latter devices automatically calculate shock waves, but at the expense of unrealistically spreading them so that continuous variation of flow properties is obtained, rather than a discontinuous jump. However, it is possible to treat shock waves explicitly as is done in the method of characteristics. The main disadvantages of the standard approaches are that the use of a rectangular net does not give the correct treatment of singularities such as centered rarefactions and the use of artificial viscosity requires that the "time step" be smaller for reasons of numerical stability, [10] thus increasing the required number of computations to obtain a given solution. With the method of characteristics, all separate waves are delineated correctly, while with the standard approach, these waves are generally diffused, thus requiring a finer mesh to obtain a given detail in the solution. Of course, the method of characteristics is logically more complicated and therefore, involves a more difficult machine coding effort while the standard approach can solve both complex and simple flows with the same ease because of the automatic handling of shock waves.

The method of characteristics is potentially more accurate than standard finite-difference approaches with artificial viscosity for the same amount of computer calculation time. However, this is at the expense of a more complicated coding effort. If a rather general method of characteristics procedure can be formulated and developed to solve arbitrary multidimensional and unsteady inviscid flows of general interest, any extra effort required for initial development and coding can be justified by the general applicability of the operational calculation procedure. Thus, rather than having to write a separate code for each flow problem, a general code can be developed to handle a large range of flow problems. This paper reports work that has been begun in the development of such a general purpose method of characteristics calculation procedure.

Notation

B function describing body surface [Eq. (22)]
h specific enthalpy
s specific entropy

β_i characteristic coordinates
γ ratio of specific heats
φ coordinate transformation matrix

Superscripts:

$( )^n$ indicates the value of a quantity at the nth iteration step

Subscripts:

$( )_{1,2,3}$ refer to the numbered points in the finite-difference network
$( )_{s,p,\varrho}$ indicates that either entropy, pressure, or density is held constant in the thermodynamic derivative

II. Summary of Equations

The equations of change for a compressible inviscid fluid which are to be solved here are:

Mass Conservation

$$\partial\varrho/\partial t + \nabla \cdot (\varrho \mathbf{V}) = 0; \tag{1a}$$

Momentum Conservation

$$\varrho(D\mathbf{V}/Dt) + \nabla p = 0; \tag{1b}$$

Energy Conservation

$$\varrho(Dh/Dt) - Dp/Dt = 0; \tag{1c}$$

Equation of State

$$h = h(p, \varrho), \tag{1d}$$

where

$$D/Dt = \partial/\partial t + \mathbf{V} \cdot \nabla.$$

Additional dependent variables can be introduced with appropriate thermodynamic relations.

$$s = s(p, \varrho), \tag{2a}$$

$$a = a(p, \varrho), \tag{2b}$$

$$T = T(p, \varrho). \tag{2c}$$

The more complex case of a nonequilibrium chemically reacting and electrically conducting fluid can be formulated, but these more complicated flows cannot

be handled with presently available computers. Therefore, only the simpler model which can be calculated with presently available computers is formulated here.

Upon substituting Eq. (1d) into (1c), the enthalpy h can be eliminated to give

$$a^2(D\varrho/Dt) - Dp/Dt = 0, \tag{3}$$

where the velocity of sound is given by

$$a^2 = -\left(\frac{\partial h}{\partial \varrho}\right)_p \left[\left(\frac{\partial h}{\partial p}\right)_\varrho - \frac{1}{\varrho}\right]^{-1} \tag{4}$$

Substituting Eq. (2a) into (3) and utilizing the fact that

$$a^2 = (\partial p/\partial \varrho)_s \tag{5}$$

gives

$$Ds/Dt = 0. \tag{6}$$

Eqs. (3) and (6) will sometimes be more useful forms of the energy conservation equation than Eq. (1c).

The general characteristic theory of hyperbolic partial differential equations is given by Courant and Hilbert [11]. Specific application of the theory to fluid mechanics problems is made by Courant and Friedrichs [12]. A clear discussion of the application of the theory to multidimensional fluid mechanics is given by von Mises [13]. The classical theory is not reiterated here. Summaries of the portions of the theory utilized in the numerical method of characteristics are given in [14] and [2].

Utilizing Cartesian coordinates (x, y, z, t), the characteristic determinant for Eqs. (1) yields the following characteristic equation.

$$\left(\frac{D\beta_1}{Dt}\right)^3 \left\{\left(\frac{D\beta_1}{Dt}\right)^2 - a^2\left[\left(\frac{\partial \beta_1}{\partial x}\right)^2 + \left(\frac{\partial \beta_1}{\partial y}\right)^2 + \left(\frac{\partial \beta_1}{\partial z}\right)^2\right]\right\} = 0. \tag{7}$$

The characteristic hypersurface is defined as

$$\beta_1(x, y, z, t) = \text{constant}, \tag{8}$$

where a transformation of coordinates of the form

$$\{\beta_1, \beta_2, \beta_3, \beta_4\} = [\varphi]\,\{x, y, z, t\} \tag{9}$$

has been introduced. Eq. (7) is a partial differential equation which leads to two sets of real characteristic hypersurfaces given by

$$D\beta_1/Dt = 0, \tag{10}$$

$$\left(\frac{D\beta_1}{Dt}\right)^2 - a^2\left[\left(\frac{\partial\beta_1}{\partial x}\right)^2 + \left(\frac{\partial\beta_1}{\partial y}\right)^2 + \left(\frac{\partial\beta_1}{\partial z}\right)^2\right] = 0. \tag{11}$$

Equation (10) corresponds to hypersurfaces made up of particle lines while Eq. (11) results in the quadratic hypersurfaces usually termed Mach hyperconoids. The latter are just the envelopes of sound waves that would appear in the fluid if a point disturbance were placed at a point in the flow. Equations (10) and (11) define the geometry of the characteristic hypersurfaces which is then used in the synthesis of the finite-difference network.

Utilizing the classical characteristic theory it is possible to derive compatibility equations for each of the characteristic hypersurfaces. These equations have the property that derivatives in a direction normal to the characteristic hypersurface do not appear. The compatibility equation corresponding to the Mach hyperconoid, Eq. (11), is

$$\begin{aligned}
&\sum_{m=2}^{4}\left\{\frac{\partial u}{\partial\beta_m}\left[\frac{\partial\beta_m}{\partial x}\frac{D\beta_1}{Dt} - \frac{\partial\beta_1}{\partial x}\frac{D\beta_m}{Dt}\right]\right.\\
&\quad + \frac{\partial v}{\partial\beta_m}\left[\frac{\partial\beta_m}{\partial y}\frac{D\beta_1}{Dt} - \frac{\partial\beta_1}{\partial y}\frac{D\beta_m}{Dt}\right]\\
&\quad + \frac{\partial w}{\partial\beta_m}\left[\frac{\partial\beta_m}{\partial z}\frac{D\beta_1}{Dt} - \frac{\partial\beta_1}{\partial z}\frac{D\beta_m}{Dt}\right]\\
&\quad + \frac{\partial p}{\partial\beta_m}\frac{1}{\varrho}\left[\frac{1}{a^2}\frac{D\beta_m}{Dt}\frac{D\beta_1}{Dt} - \left(\frac{\partial\beta_m}{\partial x}\frac{\partial\beta_1}{\partial x}\right.\right.\\
&\quad \left.\left.\left.+ \frac{\partial\beta_m}{\partial y}\frac{\partial\beta_1}{\partial y} + \frac{\partial\beta_m}{\partial z}\frac{\partial\beta_1}{\partial z}\right)\right]\right\} = 0.
\end{aligned} \tag{12}$$

Note that derivatives in the β_1-direction do not appear in (12). The particle line, Eq. (10), is a threefold characteristic so three compatibility equations are available, but only one is needed in the numerical procedure. By inspection it is seen that Eq. (1c) is a compatibility equation for the particle line because it contains substantial derivatives only. A more useful form of the equation is (6), however, which can be written in the form

$$ds/d\beta_2 = 0 \tag{13}$$

where the β_2 coordinate is chosen to lie along the particle line. Thus, Eq. (13) can be integrated to give

$$s = \text{constant (on a particle line)}, \tag{14}$$

which is the final compatibility equation that is needed.

Equations (12) and (14) are solved in the numerical method of characteristics by a finite-difference procedure. Equation (12) is put in finite-difference form by introducing the following typical approximation for a derivative.

$$\partial u/\partial \beta_2 = (u_2 - u_1)[(x_2 - x_1)^2 + (y_2 - y_1)^2 + (z_2 - z_1)^2 + (t_2 - t_1)^2]^{-1/2} \tag{15}$$

The β_2 coordinate has been chosen to lie along a line in the characteristic hypersurface from a point where the solution is known and denoted by a subscript 1 (initial data point) to a point where the solution is to be determined denoted by a subscript 2. The derivatives in the β_3- and β_4-directions are evaluated numerically by any one of a number of means. This is discussed in detail in the next section. The derivatives of the form $\partial\beta_3/\partial y$ in (12) are given by the coordinate transformation (9). This transformation is determined by requiring that (11) hold, that the β_2-direction be oriented as specified above and, for example, that the β_1 coordinates be orthogonal [14].

In order to locate the position (the x, y, z, t coordinates) of the new point at which the flow field properties are to be calculated, the intersections of certain characteristic hypersurfaces must be determined. For the purpose of determining such intersections the Mach hyperconoid is approximated locally by the Mach hypercone. The hypercone is locally tangent to the hyperconoid and its equation is easily derived from the geometry of sound waves assuming a locally uniform steady flow. The equation of the hypercone is

$$\begin{aligned}(x - x_i)^2 + (y - y_i)^2 + (z - z_i)^2 + (t - t_i)^2(u^2 + v^2 + w^2 - a^2) \\ - 2u(x - x_i)(t - t_i) - 2v(y - y_i)(t - t_i) - 2w(z - z_i)(t - t_i) = 0,\end{aligned} \tag{16}$$

where (x_i, y_i, z_i, t_i) are the coordinates of the local point under consideration.

In this section the equations needed for the numerical method of characteristics have been summarized. In the next section the numerical procedures and iteration schemes required to solve these equations are outlined and the choice of a characteristic network is discussed.

III. Outline of the Numerical Method

To keep this paper to a reasonable length the numerical method will be outlined rather than discussed in detail. Full details including program listings of the original version of the method are given in [14]. The method described here is a

modified version of the original, but the fundamental principles are the same. Also, for the sake of brevity, only the two-dimensional unsteady case will be discussed here. The actual calculations were for this case and extension to the full three-dimensional unsteady case is rather simple [14].

In applying the method of characteristics to problems of more than two independent variables the fact that characteristic surfaces are encountered rather than characteristic lines introduces an additional "degree of freedom" in the choice of the finite-difference network. This additional "degree of freedom" allows the synthesis of many different networks and indeed Fowell [15] discusses five such networks while even more have been proposed [3]. The choice of a network involves two considerations. First, it must be numerically stable and second, it should be computationally efficient. Unfortunately, neither of these considerations are simply decided.

Stability can be judged using the Courant–Friedrichs–Levy (CFL) necessary condition and the stronger, but less simply applied, von Neumann condition [3]. Both conditions rest ultimately on a heuristic approach due to the lack of an exact test for stability of nonlinear partial difference equations. The simple procedure adopted here is to apply the CFL condition to the geometry of the network and to check heuristically by calculating a known flow field.

The computational efficiency of a network is defined here as being inversely proportional to the amount of effort required to obtain numerical results. This effort involves the coding of the finite difference procedure and the amount of time and storage capacity required by the computer to obtain a result of a given degree of accuracy. This, too, is difficult to judge short of actually coding the procedures and making direct comparisons with test problems. Nearly all such judgements made before actual coding must be subjective.

Because of the difficulties in evaluating the stability and efficiency of a network and the large amount of time required to code a multidimensional procedure, the network used in this study must be said to have evolved rather than having been optimized. This does not mean that the evolutionary process could not be approaching an optimum, but that this optimum has not yet been reached. The network was termed the modified tetrahedral characteristic line network in [14], and the name is still applicable even though it has been modified further. The modifications have slightly changed the advantages and disadvantages originally cited [14], [15] for the network, but not to the extent that a different network should be chosen as the most efficient. The network for a basic field point is shown in Fig. 1.

The method of characteristics starts with data (u, v, p, s) given on an initial data surface. The solution is obtained on an adjacent surface at a later time in

the (x, y, t) space. The solution can be obtained at three different types of points at the present time. These are points in the field, points on a shock wave bounding the field, and the points on a body surface. It also is possible to obtain solutions on shock waves, rarefaction waves from body-surface corners, and contact surfaces within the field, but these procedures have not yet been coded. We will briefly describe the field, shock, and body-point procedures.

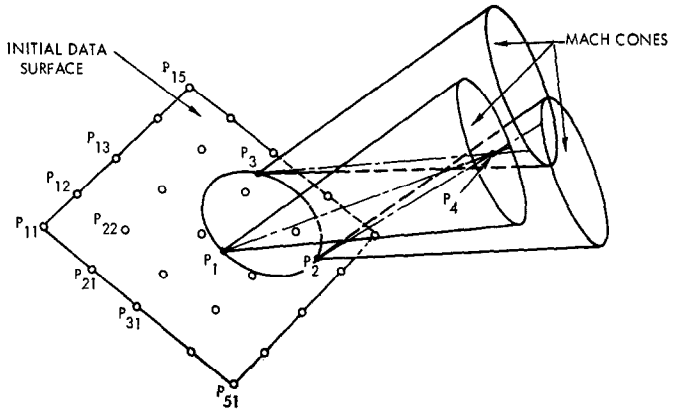

FIG. 1. The finite-difference network.

The basic field point procedure is shown in Fig. 1. First the desired location (x_4, y_4, t_4) of the new data point P_4 is determined in such a way as to keep the spacing of the data points regular. This process is discussed further below. The base points, P_1, P_2, P_3, are located in the initial data surface such that the desired location of P_4 is approximately obtained. It should be noted that, for the calculations reported here, the data surfaces were almost planar surfaces which closely approximate $t =$ constant planes. This is not necessary to the calculation, but it does make for convenience. Thus, P_1, P_2, P_3 are equally spaced on a circle in the initial data surface whose center is located at $(x_4 - u_4 \Delta t, y_4 - v_4 \Delta t, t_4 - \Delta t)$, where Δt is the desired time step size and u_4 and v_4 are approximate values of the velocity components at P_4 obtained, for example, by interpolation in the initial data surface for the point located at $(x_4, y_4, t_4 - \Delta t)$. The radius of the circle is given by $a_4 \Delta t$ where a_4 can be determined in the same way as u_4 and v_4.

Δt is limited by the CFL condition which states that the domain of dependence of the partial differential equations must be contained within the domain of dependence of the difference scheme. For Fig. 1 this means that the circle inscribed through P_1, P_2, P_3 must lie entirely within the polygon obtained by connecting

with straight lines the outermost initial data points used in the interpolation. The radius of this circle is $a\Delta t$ and thus it is seen that an upper limit is placed on Δt such that no part of the circle may fall outside of the polygon.

Now that the locations of the base points P_1, P_2, P_3 have been determined the properties at these points are determined by interpolation among the initial data points P_{ij} of Fig. 1. This is done using a 5×5 array of data points and orthogonal polynomials to give a second-degree, three-independent-variable, least-square "surface" fit to the data. The interpolation is performed with this "surface" fit. After the dependent variables (u, v, p, s) are obtained for P_1, P_2, P_3 the coordinates and these same variables for P_4 are determined. The coordinates are obtained by solving Eq. (16) written for the points P_1, P_2, P_3 $(i = 1, 2, 3)$ using the Richmond iteration procedure [16] which is accurate to third order in the step size. The compatibility equation (12) is then written for the three lines P_1P_4, P_2P_4, P_3P_4 using values for the coefficients evaluated at the base points and these equations are solved to give u_4, v_4, p_4. The derivatives in the β_3-direction are obtained in the following manner. For example, consider the u derivatives

$$\frac{\partial u}{\partial \beta_3} = \frac{\partial u}{\partial x}\frac{\partial x}{\partial \beta_3} + \frac{\partial u}{\partial y}\frac{\partial y}{\partial \beta_3} + \frac{\partial u}{\partial t}\frac{\partial t}{\partial \beta_3}. \tag{17}$$

The $\partial x/\partial\beta_3$, $\partial y/\partial\beta_3$, $\partial t/\partial\beta_3$ are obtained from the coordinate transformation, and the other partial derivatives from

$$(u_4 - u_i) = \frac{\partial u}{\partial x}(x_4 - x_i) + \frac{\partial u}{\partial y^2}(y_4 - y_i) + \frac{\partial u}{\partial t}(t_4 - t_i) \quad (i = 1, 2, 3). \tag{18}$$

At the first step in the iteration, u_4 can be approximated as

$$u_4 = \tfrac{1}{3}(u_1 + u_2 + u_3). \tag{19}$$

The entropy s is determined by projecting the particle line back from P_4 to obtain its intersection with the initial data surface and interpolating among the points on the initial data surface as before because the entropy is constant along the particle line.

Finally, the solution of Eqs. (12) and the projecting of the particle line is repeated in an iteration procedure where average values of the coefficients in the equations are used instead of the values at the base points. These averages are taken between the appropriate base point and the new point. This procedure is similar to the modified Euler's method which is sometimes referred to as Heun's first method for ordinary differential equations [16]. When applied to ordinary differential equations, the truncation error is third-order in the step size. The procedure as

applied here to the partial differential equations, does omit some terms which are second-order in the step size through the assumption that the partial derivatives in Eq. (18) are constant over the network. The only way to overcome this deficiency is to introduce a more elaborate method to numerically evaluate the derivatives in the β_3-direction.

The calculation of the solution at a point on a bounding shock wave is similar to the procedure for a field point, but differs in a few details. First, one of the base points, P_3 say, must be located on the shock wave. For each such shock point in addition to the usual dependent variables (u, v, p, s) the components of the shock wave surface unit normal vector, N_x, N_y, N_t, must be available. The shock wave is approximated locally as a plane passing through the shock point and lying normal to the unit normal vector. The other two base points, P_1 and P_2, are again field points located on the circle which is the intersection of the Mach cone through the new shock point with the initial data surface. The positioning of these points and interpolation to obtain the dependent variable is the same as in the field-point procedure. The coordinates of the new shock point are determined by finding the intersection of the two Mach cones with the plane which is the local approximation to the shock wave. Next, the shock-wave equations can be solved to give the flow properties behind the shock at the new shock point, [14] but these properties do not necessarily satisfy the two compatibility equations, (12), that can be written for the lines P_1P_4 and P_2P_4. Thus the dependent variables are expanded in Taylor series in the following form:

$$u_4^{(n+1)} = u_4^{(n)} + \left(\frac{\partial u_4}{\partial N_{x_4}}\right)^{(n)} \Delta N_{x_4}^{(n)} + \left(\frac{\partial u}{\partial N_{y_4}}\right)^{(n)} \Delta N_{y_4}^{(n)} \tag{20}$$

where the superscripts refer to the iteration cycle and ΔN_{x_4} is the correction required to the x-component of the unit normal vector in order to satisfy the compatibility equations. The derivatives in (20) are obtained from the shock wave equations. When (20) together with similar expressions for v and p are substituted into the two compatibility equations, they can be solved for ΔN_{x_4} and ΔN_{y_4}. Note that ΔN_{t_4} can be obtained from

$$(N_x + \Delta N_x)^2 + (N_y + \Delta N_y)^2 + (N_t + \Delta N_t)^2 = 1 \tag{21}$$

after the other two corrections have been determined. The entire process is then repeated using average values for the coefficients in the equations just as in the field point iteration procedure.

The third type of point that is calculated is a point lying on the body surface. This procedure is very similar to the shock point procedure discussed above. One

of the base points is located on the body. In contrast to the shock point, body-surface unit normal vector components are not specified for the body points. The body is described by a function of the form

$$B(x, y, t) = 0. \tag{22}$$

All references to this function in the program are combined into one subroutine. Then, in order to specify a different body motion, only this single subroutine need be changed. The body surface is still treated locally as a plane which is taken as the plane of tangency of the surface, Eq. (22), at the point being considered. As in the shock point, the new body point is located at the intersection of two Mach cones from base points in the field with the plane tangent to the body surface at the body base point. The two compatibility equations for the base points in the field are solved simultaneously with the boundary condition that fluid does not pass through the body surface,

$$\frac{\partial B}{\partial x} u + \frac{\partial B}{\partial y} v + \frac{\partial B}{\partial t} = 0. \tag{23}$$

This determines u, v, and p. Entropy s is determined as in the field point by projecting the particle line back to its intersection with the initial data surface and interpolating. The process is then repeated using average values for the coefficients in the equations in an iteration process just as in the field and shock points.

The three basic elements of calculating field, shock, and body points must be combined in a master program to calculate a complete flow field. The organization of this program is outlined next. First, the size of the time step, Δt, must be determined. This is done by searching the net of points to find the maximum Δt which does not violate the CFL condition. Then a Δt of 0.75 of this maximum is used. The factor 0.75 is a safety factor to ensure stability.

Half of the complete net of points used to calculate the blunt body flow discussed in the next section is shown in Fig. 2. This shows the (x, y)-locations of points in the initial data plane. The basic calculation unit is the 5×5 array of points shown in the center of Fig. 2 outlined by the solid line. The initial data is fitted with the orthonogonal polynomial procedure over this 5×5 array. New field points on the next $t =$ constant surface, with (x, y)-locations close to those indicated by the six flagged points inside the array, are calculated using the same interpolation fits. These six particular points are chosen such that their domains of dependences (the circle inscribed through P_1, P_2 and P_3 in Fig. 1) lie closest to the center of the 5×5 array. On the edges of the net the fits are used for more than six points as shown by the outlined area in the right-hand corner of the net

in Fig. 2. Here the nine flagged points indicate those points which are used with the same interpolation fit. Note that even though points on the edge of the fitted area are calculated the CFL condition is not violated because the flow is supersonic in this area and hence the domains of dependence are well within the interpolation area.

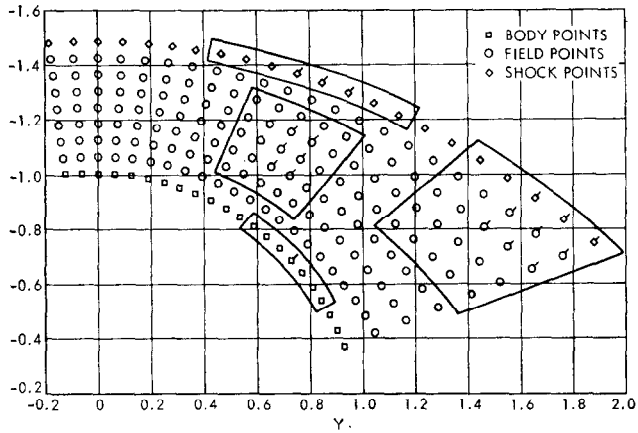

FIG. 2. Organization of the calculation procedure.

Interpolations for properties along the shock wave and body require single independent variable fits of second degree. A basic array of seven points is used for the interpolation at a single central point as shown for the body points at the bottom of Fig. 2. A fit over eight points is used for the interpolation at three shock points as shown at the top of the figure. These interpolations are used to determine s for the body points and N_x, N_y, N_t and other properties for the shock points.

The master program controls the calculation by sequentially stepping through the net, fitting the 5×5 arrays of points, and calculating the new points on the next data surface. The desired (x, y)-location of the new points is obtained by equally distributing the seven field points along the ray from a body point to a corresponding shock point. In this way, for steady flow the existing order in the net is maintained and in unsteady distorting flows some degree of order is retained.

Various other refinements have been added to the calculation procedure which are not absolutely necessary to obtain successful results, but improve either the form or accuracy of the results. For example, it was found desirable to add some active adjustment to the procedure in order to try to retain almost planar $t =$ constant data surfaces. Thus, at a particular time step, an average time is computed

and the diameter of the base circle through P_1, P_2, P_3 in Fig. 1 is proportionally increased (decreased) slightly when the time of the point with the desired (x, y) coordinates in the initial data surface is less (greater) than the average time for the initial data surface. This actively controls the t-coordinates of the points.

Another refinement has to do with the location of the base points in the field. In Fig. 1, P_1, P_2, and P_3 can be located arbitrarily around the circle. It was found by numerical experiments that higher accuracy is obtained by spacing them evenly about the circle, but this still leaves a single degree of freedom in orienting the points. It was found that higher accuracy could be obtained by doing the calculation twice, once with the set of points indicated by circles in Fig. 3(a) and once with the set indicated by squares, and then averaging the two results. The improvement in accuracy in this case is mainly in the reduction of the shock wave velocity drift [see the discussion of Fig. 5(b) in the next section] by as much as a factor of two and through better control of the (x, y)-positions of the points. This procedure was suggested by the work of Strom [5]. Actually, the calculation does not take twice as long as when only one set of base points is used, because when the second calculation is performed the reults of the first calculations are used as initial estimates and these are very good; so only a few more iterations are necessary to converge the second calculation. Two sets of field base points are also used in the same way for the shock point. The same shock base point is used, however. It has been found experimentally, that the highest accuracy is obtained by locating the points asymmetrically relative to the shock wave as shown in Fig. 3(b). A similar study was done for the body point. It was found that the field base points should be symmetrically located relative to the body, but, in trying

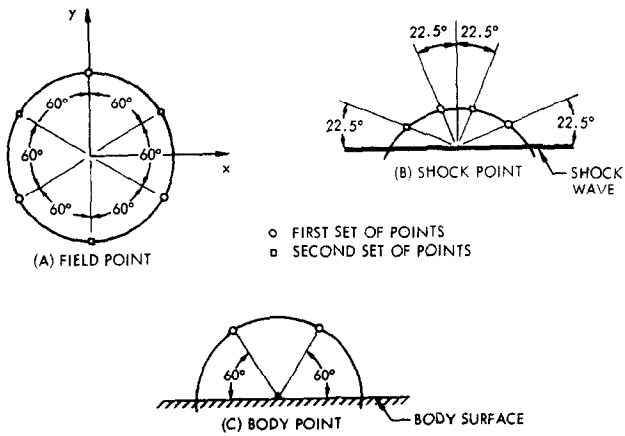

FIG. 3. Location of base points in the field.

to determine the best location of the two sets of points, opposing accuracy requirements were found. u, v, and p could be made more accurate at the expense of accuracy in x, y, and t or vice versa, so the best compromise was found to be a single set of points located uniformly as shown in Fig. 3(c).

This completes the outline of the numerical method and the organization of the program. Of course, many details such as the form of input and output both digital and graphical cannot be taken up here and probably should be tailored to the particular type of flow under consideration and the type of computation facilities being used.

IV. Results of Recent Calculations

The calculations reported on in this section were carried out on an IBM 7094 II direct coupled to a 7040 for input and output. Graphical results were plotted off-line on a 1627 plotter.

All flow fields calculated here started with the same data on the initial data surface, $t = 0$. This data was obtained from the work of Belotserkovskii [17] where it was calculated by the method of integral relations using two strips. This initial flow is for a perfect gas ($\gamma = 1.4$) at conditions approximately equivalent to an altitude of 50 000 feet with a freestream Mach number of 5. The body surface is a circular cylinder with its axis normal to the freestream velocity. The data was given by Belotserkovskii for the net shown in Fig. 2 except that only three evenly spaced rings of field points were given. The four additional rings of field

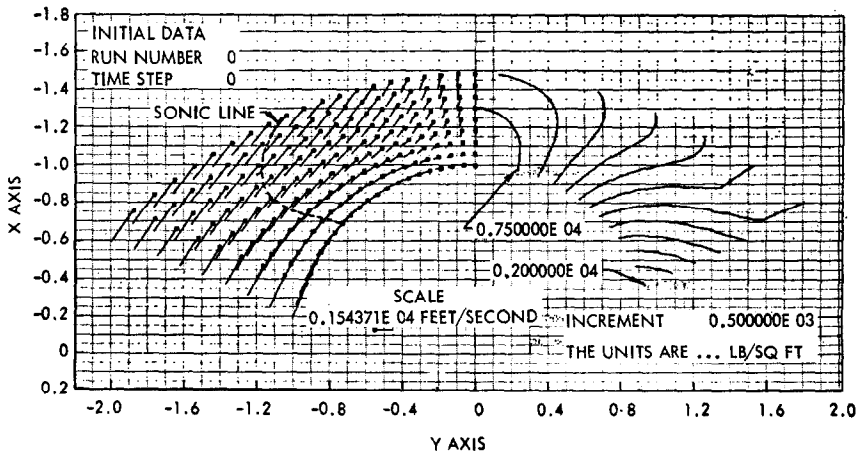

Fig. 4. Initial data.

points were added by interpolation using the second-degree orthogonal polynomial procedure mentioned above. The original Belotserkovskii data was given to three and in a few cases four decimal digits. The calculations were performed using mainly single precision arithmetic (eight decimal digits) though in a few places where accuracy was found to be important double precision was used. The iterations were generally converged to five digits. This initial data is shown in Fig. 4 where on the left the velocity vector field is shown and on the right the pressure field. Note that there are no arrowheads on the velocity vectors and the squares marking the location of the data points are at the base of the vectors. Only the maximum and minimum pressure contours are labeled. The increment from one contour to the next is 500 lb/ft.^{2}, as given on the figure. All velocity vector and pressure-field plots in this paper were directly generated by the computer.

The results of two flow calculations are reported in this paper. Many others have been calculated and more calculations of this sort are planned in an effort of continuing improvement and application of the method.

The original version of the program was checked for errors using simple one-dimensional cases and against hand calculations. This gave assurance that no major bugs were in the program and that the finite-difference approach was sound. No method of characteristics procedure or finite-difference solution is completely free of errors. There are roundoff and truncation errors in all finite-difference procedures. Due to these errors, the method of characteristics does not *exactly* conserve mass, momentum, and energy. There are means of estimating these errors [18], [19], and correcting them [20] if this becomes necessary. No such corrections have as yet been undertaken in this work. A very simple way to gain an estimate of these errors is to make a calculation in which the body surface is held constant in time and then check on how fast the solution at later times "drifts" away from the initial steady-state solution. This gives an estimate of the rate of growth of errors in the calculation procedure.

The first calculation reported here was just such a steady-flow check, and 45 time steps were calculated. It has been found that the most sensitive indicators of this drift error are the stagnation pressure and the velocity of the shock wave. Plots of these indicators are shown in Fig. 5. In Fig. 5(a) it can be seen that the average rate of increase of the stagnation pressure is 0.15% per time step. This can be compared to a rate of decrease of 2.0% per time step in the original version of the method which used linear interpolation throughout. Thus the change from linear to second-degree interpolation contributed to an order-of-magnitude decrease in the error. In Fig. 5(b) note that even though the shock-wave velocity has reached 826 ft./sec., this is not extremely large when it is considered that a V_s of 100 ft./sec. corresponds to an N_t of only 0.05 in the present calculation.

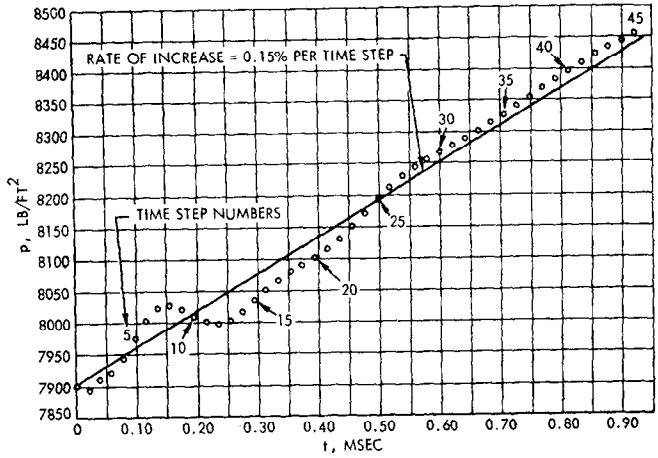

FIG. 5(a). Stagnation point pressure drift for steady flow.

Thus, the shock-wave velocity is quite sensitive to errors and is an area where accuracy improvement can be quite beneficial. Also, note that for the short time scale of approximately 1 msec. the shock wave does not move very far even for these higher velocities. The extent of the shock-wave movement can be seen in

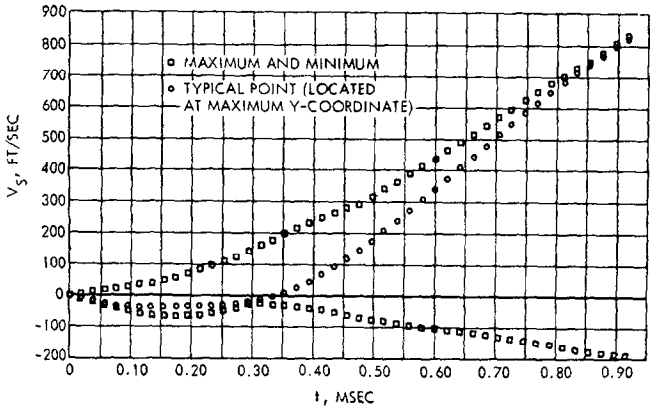

FIG. 5. (b) Shock-wave velocity drift for steady flow.

Fig. 6, where the initial shock-wave location can be compared with its location at time step 38. The distortion in the velocity field can be judged by comparing Figs. 6 and 4. Figure 7 gives an indication of the amount of drift in the pressure field. Note that the drift is largest near the stagnation point as mentioned above.

A comment on computation time and calculated flow time might be appropriate at this point. First of all, the calculation requires approximately three minutes of computer time per time step for this 351-point net. The time is relatively independent of the body motion considered. With linear interpolation and by omit-

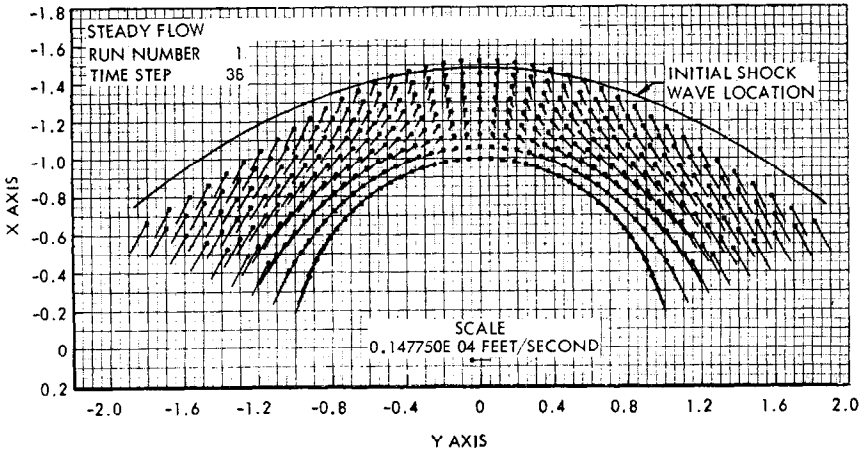

FIG. 6. Steady-flow velocity field at time step 38.

ting many of the refinements discussed in the previous section, the calculation required approximately 1.7 min per time step for the same net of points. The programs to perform the calculation and the flow field data for 351 points approximately fill the 32 000-word magnetic-core storage of the machine so that the

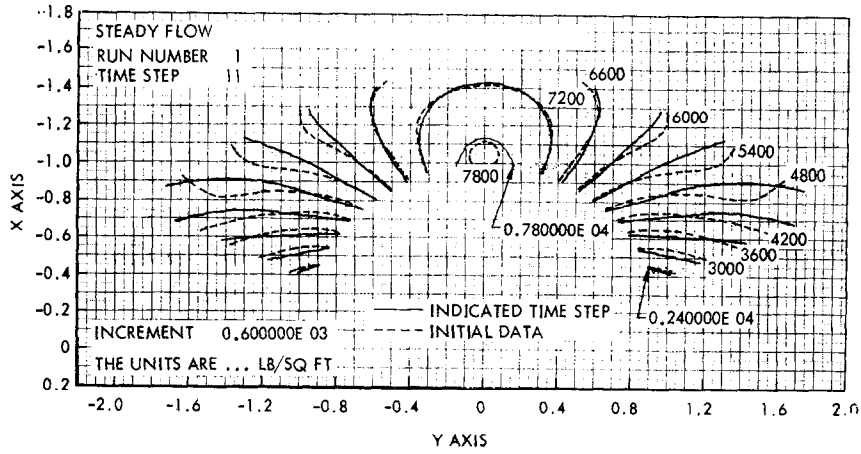

FIG. 7(a). Steady-flow pressure field.

graphical plotting programs must be run separately after the calculation. Usually three different plots are made for each time step and these require approximately 10 sec per plot. Thus, the steady-flow run of 45 time steps required approximately 2 h, 37 min, 30 sec of computer time.

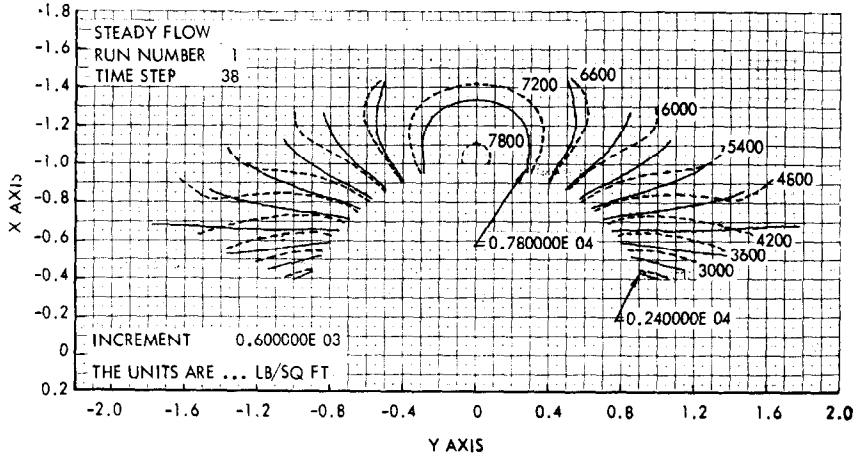

FIG. 7 (b). Steady-flow pressure field.

The calculated flow time is arbitrary as to its zero point and, to some extent, its scale. In Fig. 5 the initial data is shown to be at $t = 0$. In the calculation it was found convenient for reasons of numerical accuracy to multiply the real time by a constant velocity to make the dimensions of t the same as the dimensions of the space coordinates and to give t the same numerical order of magnitude as the space coordinates. This velocity was chosen to be 2000 ft./sec. in the calculations reported here. It was also found advantageous for reasons of numerical accuracy to perform all calculations at a transformed "time" of 0.3 ft. Thus, just before a new time step was calculated, an average time for all the data points was determined and this average, less 0.3, was subtracted from the time coordinate of all points. After the calculation the average, less 0.3, was added to the time coordinate.

The second calculation presented here is an unsteady flow where the circular cross section of the cylinder is warped to an ellipse whose semimajor axis is 7% greater than the radius of the cylinder. The semimajor axis of the ellipse grows in time using one-half the period of a cosine function displaced by one-half its amplitude. This axis is located at an angle of attack of 20°. The equations for the motion of the body surface are

$$B(x, y, t) = \frac{4\{x^2 \cos^2 \alpha - xy \sin 2\alpha + y^2 \sin^2 \alpha\}}{\{(A-1)\cos[\pi(1 + t/t_0)] + A + 1\}^2}$$

$$+ x^2 \sin^2 \alpha + xy \sin 2\alpha + y^2 \cos^2 \alpha - 1 = 0 \text{ for } 0 \leq t \leq t_0, \quad (24a)$$

$$B(x, y, t) = x^2\left(\frac{\cos^2 \alpha}{A^2} + \sin^2 \alpha\right) + xy\left(1 - \frac{1}{A^2}\right)\sin^2 \alpha$$

$$+ y^2\left(\frac{\sin^2 \alpha}{A^2} + \cos^2 \alpha\right) - 1 = 0 \quad \text{for} \quad t > t_0, \quad (24b)$$

where for this case $\alpha = 20°$, $A = 1.07$, $t_0 = 0.15$ msec. The body motion is stopped for $t > 0.15$ msec, which falls between time steps 9 and 10.

Figure 8 shows the pressure on the body surface at $y \approx 0$ and the maximum and minimum shock-wave velocities as functions of time. In Fig. 8(a) it is seen that

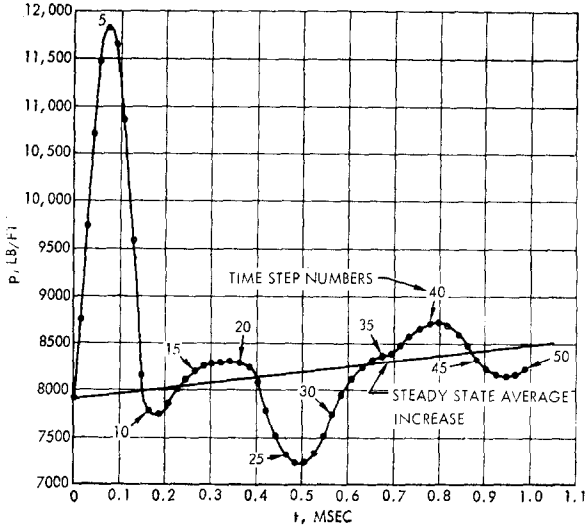

FIG. 8(a). Body-surface pressure at $y \approx 0$ for unsteady flow.

the pressure rises rapidly to a peak as the body pushes into the flow and falls rapidly again as the body motion stops. Waves then continue to reverberate back and forth between the body and the shock as the disturbance decays to a new steady state. Note [in Fig. 8(a)] the unsteady flow pressure might be oscillating about the increasing steady state average value of pressure at that point. Of course, there is no reason to assume that this should be the case because the error growth

need not be the same rate or even in the same direction for these two different cases.

Fifty time steps were carried out in this calculation. There is no reason why this calculation or the steady-flow case could not have been carried further in time. However, it was felt that due to the accumulating error the solution beyond 50 time steps would be of little value.

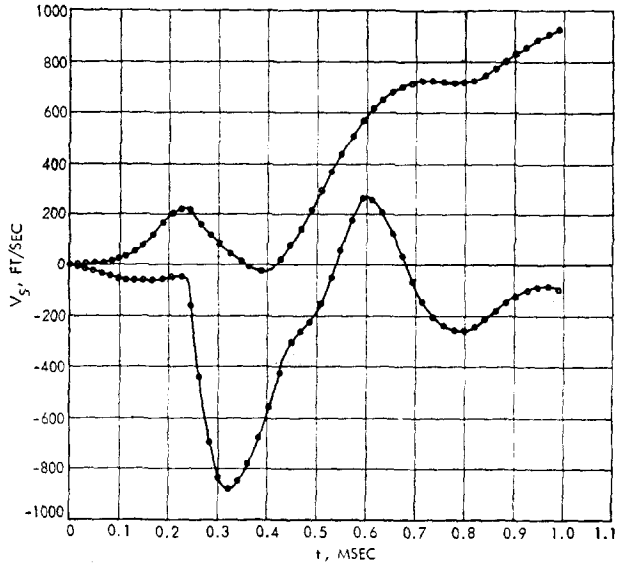

FIG. 8(b). Maximum and minimum shock-wave velocities for unsteady flow.

The shock-wave velocity is in a direction normal to the shock wave in a constant time plane. The positive sense is toward the body so a positive shock-wave velocity corresponds to the shock wave moving toward the body. There is an anomalous first motion of the shock toward the body at $t = 0.2$ msec [in Fig. 8(b)]. This is explained below. The shock then moves very quickly away from the body as is to be expected. It then proceeds to oscillate until, at $t = 0.7$ msec, the maximum velocity appears to hit a plateau and then continues to slowly rise. This seems to correspond to the point where the steady-state shock velocity would have the same value [see Fig. 5(b)]. Thus, one possible explanation could be that the "physical signal" becomes lost in the growing "noise" at this point.

Figure 9 shows the pressure at the data points closest to $y = 0$. As can be seen from Fig. 10 these points are very close to the axis, but do not lie exactly on it and are not in an exactly straight line. This accounts for some of the irregularity

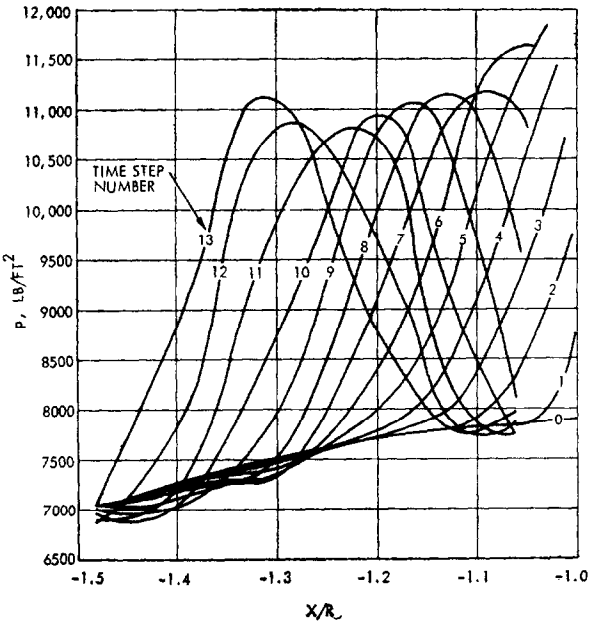

FIG. 9(a). Pressure along $y \approx 0$; unsteady flow.

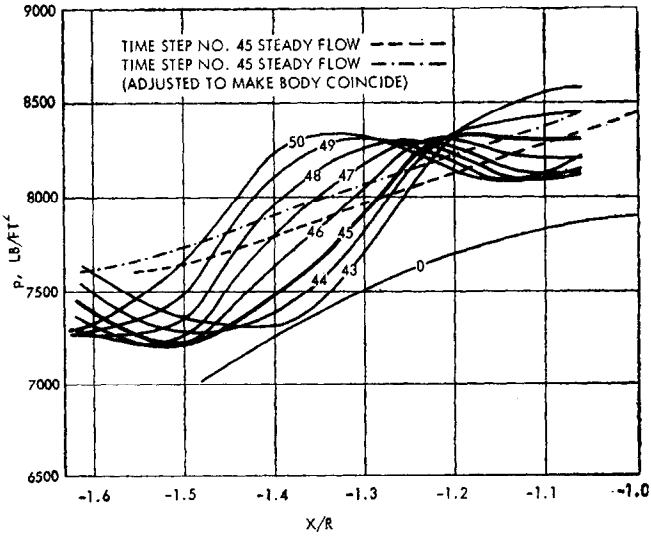

FIG. 9(b). Pressure along $y \approx 0$; unsteady flow.

in the curves of Fig. 9. As can be seen in Fig. 9(a), the compression wave leaves the body and propagates toward the shock. The reason for the anomalous initial behavior of the shock wave in Fig. 8(b) can be seen in Fig. 9(a). Note how the pressure immediately in front of strong compression wave actually falls below

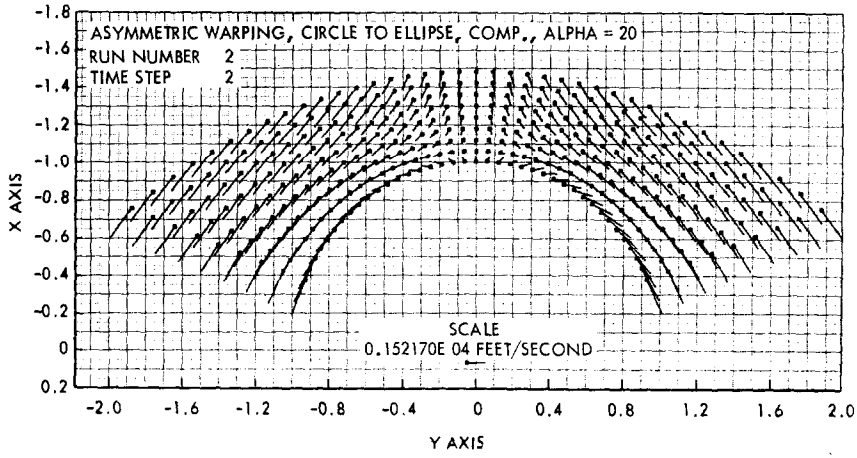

FIG. 10 (a). Unsteady-flow velocity field.

its initial value. When this small expansion reaches the shock just before the compression, it causes the shock to move initially toward the body. This is caused by the fitting of the sharp-edged compression wave, which actually has a discon-

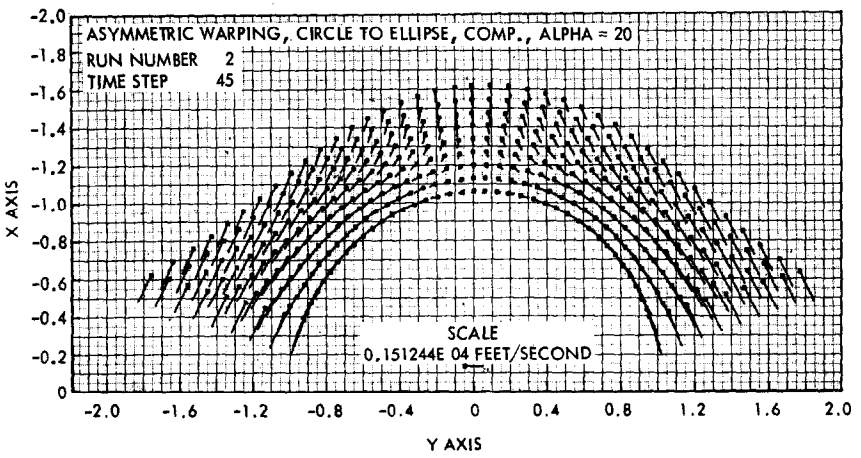

FIG. 10(b). Unsteady-flow velocity field.

tinuity in the first derivative of the dependent variables at its leading edge, with continuous second-degree polynomials and thus introducing interpolation errors. This could be alleviated by adding more points to the net between the body and the shock in order to obtain better resolution of the waves.

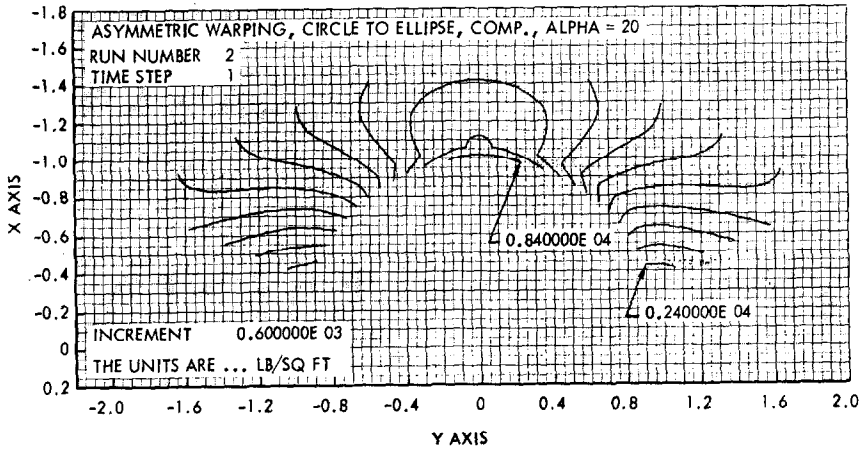

FIG. 11(a). Unsteady-flow pressure field.

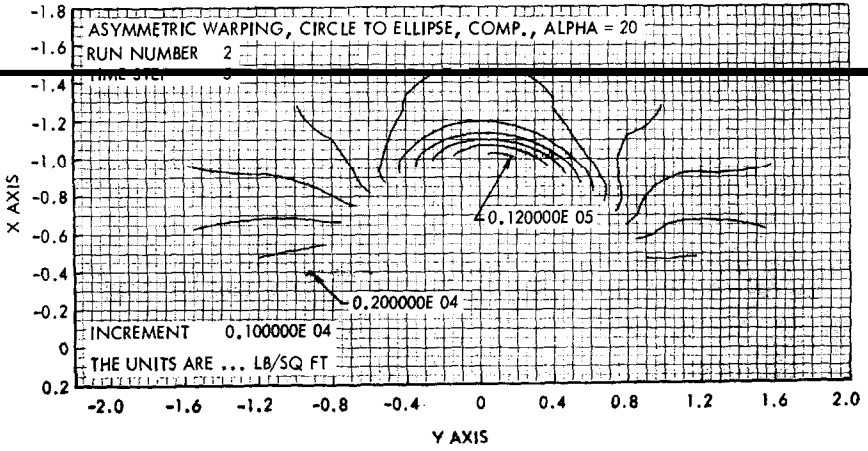

FIG. 11(b). Unsteady-flow pressure field.

In Fig. 9(b) the results for the steady flow are also plotted. Note that after the steady-flow results are adjusted to make the body surfaces coincide it appears that the unsteady solution is oscillating with decreasing amplitude about this

steady result. Also note that the same may be true of the shock standoff distance, which is to be expected for this mild change in body geometry. It appears that the unsteady calculation should reach a steady state in something less than 50 more time steps.

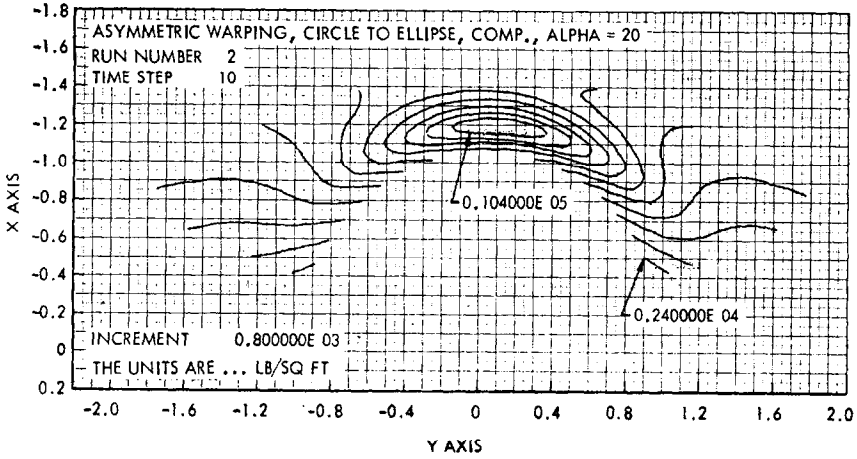

FIG. 11(c). Unsteady-flow pressure field.

Typical velocity vector fields for the unsteady flow are shown in Fig. 10. The pressure field is given in Fig. 11. The waves are readily seen in the pressure plots. Note, too, in this case, that not much asymmetry is introduced into the flow field by the 20° angle of the attack and 7% semimajor-axis growth.

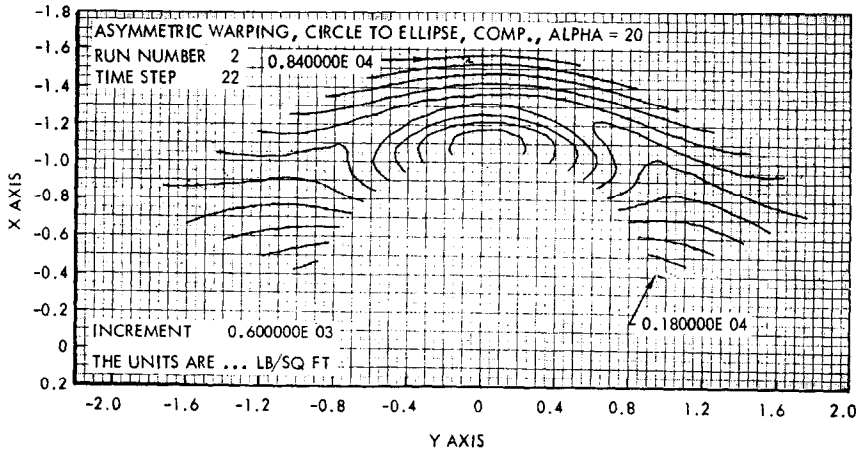

FIG. 11(d). Unsteady-flow pressure field.

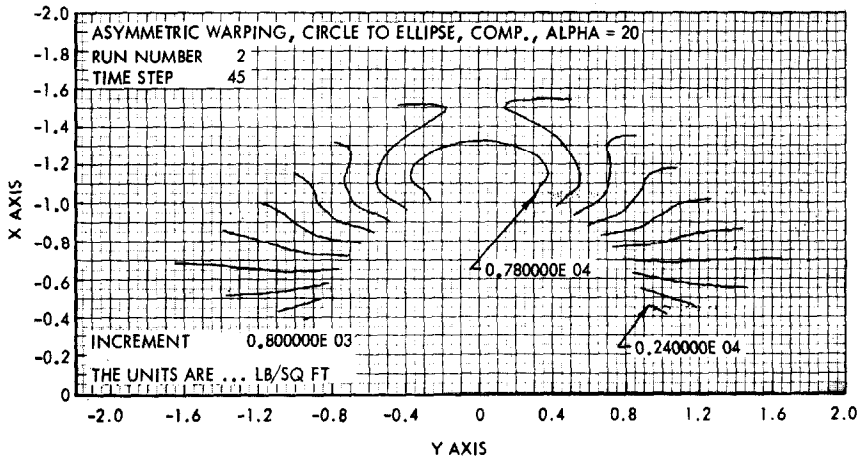

FIG. 11 (e). Unsteady-flow pressure field.

V. CONCLUSIONS

From the results of this effort it can be concluded that practical calculations of two-dimensional unsteady flows and, in general, calculations of three-independent-variable problems can be accomplished with an extensive programming effort and a reasonable amount of computer time on presently available machines. The calculation of four-independent-variable problems, at least for the simpler cases, should become feasible with the next generation of computers. These conclusions apply to general flow fields because the approach to the method of characteristics described here is not oriented to a particular flow geometry.

The results presented here show an order of magnitude decrease in error growth rate over the original version of the procedure of [14]. The size of the time step was increased fourfold while still maintaining numerical stability, and positive control of the location of the data points in the net was established. These improvements were made without resorting to formal error-correcting procedures such as those of [20].[1] Of course, higher accuracy can be obtained on the next generation of computers by using more data points in the net and higher-precision arithmetic.

[1] Further improvements in accuracy have been obtained in recent calculations performed after this paper was submitted for publication. They were accomplished by iterating the calculations to make each time step more nearly a constant time plane and by using smoothing techniques to reduce the shock-wave velocity drift. The details of these improvements will be reported later.

It appears that there are many interesting problems which can be solved with the multidimensional method of characteristics. For example, the unsteady-flow results given here suggests that steady, asymmetric blunt-body flows can be solved by considering an unsteady warping of the body surface from a simple shape to a more interesting one. It should be pointed out that the application of the present procedure to three-dimensional steady supersonic flow might be even more interesting because many problems in this area require less than 50 calculation steps and the procedure in its present form can be applied directly.

Acknowledgment

Many persons helped in the development and checking of the computer coding of the method. In particular, acknowledgement is due Mark Sussman who assisted the author in coding the original version of the method. John Szabo converted the programs from FORTRAN II to FORTRAN IV and coded the graphical output portion of the project. Dr. Morris Weisfeld supplied the orthogonal polynomial fitting routines used in the interpolation. Special thanks is given to Michael Diethelm who coded the latest version of the method and who also contributed many useful suggestions toward improving the numerical procedures.

References

1. H. SAUERWEIN, "A general Numerical Method of Characteristics," Report TDR-469, Aerospace Corporation, San Bernardino, California (1964); Paper No. 65-25, American Institute of Aeronautics and Astronautics, New York (1965).
2. H. SAUERWEIN, *J. Fluid Mech.* **25**, 17–41 (1966).
3. H. HEIE and D. C. LEIGH, *AIAA J.* **3**, 1099–1103 (1965).
4. R. SAUER, Numerische Mathematik **5**, 55–67 (1963).
5. C. R. Strom, "The Method of Characteristics for Three-Dimensional Steady and Unsteady Reacting Gas Flow," Thesis, University of Illinois (1965).
6. D. J. RICHARDSON, pp. 295–318 in Ref. [7].
7. B. ALDER, S. FERNBACH, and M. ROTENBERG (Ed.) "Methods in Computational Physics," Vol. 3. Academic Press, New York (1964).
8. J. VON NEUMANN and R. D. RICHTMYER, *J. Appl. Phys.* **21**, 232–237 (1950).
9. P. D. LAX, *Commun. Pure Appl. Math.* **7**, 159–193 (1954).
10. N. E. HOSKIN, pp. 265–293, in Ref. [7].
11. R. COURANT and D. HILBERT, "Methods of Mathematical Physics," Vol. II, Chap. 6. Interscience, New York (1962).
12. R. COURANT and K. O. FRIEDRICHS, "Supersonic Flow and Shock Waves," p. 37. Interscience, New York (1948).

13. R. VON MISES, "Mathematical Theory of Compressible Fluid Flow," p. 103. Academic Press, New York (1958).

14. H. SAUERWEIN, "The Calculation of Two- and Three-Dimensional Inviscid Unsteady Flows by the Method of Characteristics," Thesis, M.I.T., (1964) [M.I.T. Fluid Dynamics Laboratory Report. No. 64–4, AFOSR 64–1055 (1964).]

16. L. LAPIDUS, "Digital Computation for Chemical Engineers," pp. 88 and 292. McGraw-Hill, New York (1962).

17. O. M. BELOTSERKOVSKII, *Vychis. Mat.* **3**, 149–185 (1958).

18. M. G. HALL, *Quart. J. Mech. Appl. Math.* **9**, 320–333 (1956).

19. L. VEIDINGER, *Magyar Tud. Akad. Mat. Kutató Int. Közl.* **6**, 323–331 (1961).

20. S. A. POWERS and J. B. O'NEILL, *AIAA J.* **1**, 1693–1694 (1963).